Inorganic Chemistry

Article

pubs.acs.org/IC

De Novo Design and Characterization of Copper Metallopeptides Inspired by Native Cupredoxins

Jefferson S. Plegaria,[†] Matteo Duca,[§] Cédric Tard,[§] Thomas J. Friedlander,[†] Aniruddha Deb,[†,‡] James E. Penner-Hahn,[†,‡] and Vincent L. Pecoraro*[,†]

[†]Department of Chemistry and [‡]Biophysics Department, University of Michigan, Ann Arbor, Michigan 48109, United States

[§]Laboratoire d'Electrochimie Moléculaire, UMR 7591, CNRS, Université Paris Diderot, Sorbonne Paris Cité, 15 Rue Jean Antoine de Baïf, F-75205 Paris Cedex 13, France

Supporting Information

ABSTRACT: Using *de novo* protein design, we incorporated a copper metal binding site within the three-helix bundle α_3D (Walsh et al. *Proc. Natl. Acad. Sci. U.S.A.* **1999**, 96, 5486−5491) to assess whether a cupredoxin center within an α-helical domain could mimic the spectroscopic, structural, and redox features of native type-1 copper (CuT1) proteins. We aimed to determine whether a CuT1 center could be realized in a markedly different scaffold rather than the native β-barrel fold and whether the characteristic short Cu−S bond (2.1−2.2 Å) and positive reduction potentials could be decoupled from the spectroscopic properties ($\varepsilon_{600\ nm}$ = 5000 M^{-1} cm^{-1}) of such centers. We incorporated 2HisCys(Met) residues in three distinct α_3D designs designated core (CR), chelate (CH), and chelate-core (ChC). XAS analysis revealed a coordination environment similar to reduced CuT1 proteins, producing Cu−S(Cys) bonds ranging from 2.16 to 2.23 Å and Cu−N(His) bond distances of 1.92−1.99 Å. However, Cu(II) binding to the CR and CH constructs resulted in tetragonal type-2 copper-like species, displaying an intense absorption band between 380 and 400 nm (>1500 M^{-1} cm^{-1}) and $A_{\|}$ values of (150−185) × 10^{-4} cm^{-4}. The ChC construct, which possesses a metal-binding site deeper in its helical bundle, yielded a CuT1-like brown copper species, with two absorption bands at 401 (4429 M^{-1} cm^{-1}) and 499 (2020 M^{-1} cm^{-1}) nm and an $A_{\|}$ value ∼30 × 10^{-4} cm^{-4} greater than its native counterparts. Electrochemical studies demonstrated reduction potentials of +360 to +460 mV (vs NHE), which are within the observed range for azurin and plastocyanin. These observations showed that the designed metal binding sites lacked the necessary rigidity to enforce the appropriate structural constraints for a Cu(II) chromophore (EPR and UV−vis); however, the Cu(I) structural environment and the high positive potential of CuT1 centers were recapitulated within the α-helical bundle of α_3D.

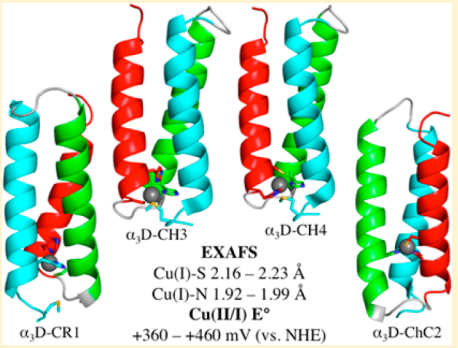

INTRODUCTION

Electron transfer (ET) is the simplest chemical transformation in a redox reaction and serves a central role in numerous bioenergetic processes including photosynthesis and respiration.[1,2] Found in bacteria, algae, plants, and animals, cupredoxins or type-1 copper centers (CuT1) are electron transfer proteins that have been extensively studied to understand this fundamental reaction.[3−6] The copper ion is encompassed in a Greek β-barrel fold and coordinated to three equatorial ligands, formed by two N(His) and one S(Cys), as well as one or two more weakly bound axial ligands, such as S(Met) or O(Gln), to form a three- to five-coordinate copper complex. The canonical CuT1 proteins give rise to unique spectroscopic, structural, and redox properties.[7,8] For example, plastocyanin and azurin display an LMCT transition at 600 nm (3000−6000 M^{-1} cm^{-1}), a compressed EPR hyperfine coupling constant ($A_{\|}$) (<70 × 10^{-4} cm^{-1}), a short Cu−S(Cys) bond of 2.1−2.2 Å, and highly positive reduction potentials ($E°$) of +180 to +800 mV (vs NHE). Green copper centers stellacyanin and the CuT1 center in copper nitrite reductase are characterized as perturbed blue copper centers with an additional LMCT band at ∼450 nm (3000−6000 M^{-1} cm^{-1}). Nitrosocyanin, a red copper center, is a recent addition to the CuT1 family and possesses the most perturbed copper site, exhibiting an inverted absorption spectrum with a λ_{max} at 390 nm (7000 M^{-1} cm^{-1}), as well as a large $A_{\|}$ (144 × 10^{-4} cm^{-1}), a Cu(II)−S(Cys) bond that is elongated by ∼0.1 Å, and a reduction potential of +84 mV.[56] This red copper center possesses the characteristics of a type-2 copper site (CuT2) or a "normal" copper center such as $Cu(II)Cl_4$.[7]

Protein design has proven to be an effective strategy for examining the metal active sites of native metalloproteins.[9−12] This biologically relevant approach has two central design strategies: the first is protein redesign/reengineering,[9] and the second is *de novo* design.[10−12] The second strategy employs first-principles to design an original sequence that forms the proper hydrophobic, electrostatic, and hydrogen-bonding

Received: June 12, 2015
Published: September 18, 2015

DOI: 10.1021/acs.inorgchem.5b01330
Inorg. Chem. 2015, 54, 9470−9482

Table 1. Amino Acid Sequence of α_3D and Redesigned α_3D Constructs[a]

peptide	sequence				metal binding site
α_3D	MGSWAEFKQR	LAAIKTR	LQAL	GGS	
	EAELAAFEKE	IAAFESE	LQAY	KGKG	
	NPEVEALRKE	AAAIRDE	LQAYRHN		
α_3DIV	MGSWAEFKQR	LAAIKTR	**C**QAL	GGS	C18, C28, C67
	EAE**C**AAFEKE	IAAFESE	LQAY	KGKG	
	NPEVEALRKE	AAAIRDE	**C**QAYRHN		
α_3DH$_3$	MGSWAEFKQR	LAAIKTR	**H**QAL	GGS	H18, H28, H67
	EAE**H**AAFEKE	IAAFESE	LQAY	KGKG	
	NPEVEALRKE	AAAIRDE	**H**QAYRVNGSGA		
α_3D-CR1	MGSWAEFKQR	LAAIKTR	**H**QAL	GGS	H18, C28, H67, M72
	EAE**C**AAFEKE	IAAFESE	LQAY	KGKG	
	NPEVEALRKE	AAAIRDE	**H**QAYR**M**NGSGA		
α_3D-CH1	MGSWAEFKQR	LAAIKTR	**H**QA**H**	GGS	H18, H21, C28, M72
	EAE**C**AAFEKE	IAAFESE	LQAY	KGKG	
	NPEVEALRKE	AAAIRDE	LQAYR**M**NGSGA		
α_3D-CH2	MGSWAEFKQR	LAAIKTR	**H**QAL	**C**GS	H18, C22, H28, M72
	EAE**H**AAFEKE	IAAFESE	LQAY	KGKG	
	NPEVEALRKE	AAAIRDE	LQAYR**M**NGSGA		
α_3D-CH3	MGSWAEFKQR	LAAIKTR	**H**QA**C**	GGS	H18, C21, H28, M72
	EAE**H**AAFEKE	IAAFESE	LQAF	KGKG	
	NPEVEALRKE	AAAIRDE	LQAFR**M**NGSGA		
α_3D-CH4	MGSWAEFKQR	LAAIKTR	**C**QA**H**	GGS	C18, H21, H28, M72
	EAE**H**AAFEKE	IAAFESE	LQAF	KGKG	
	NPEVEALRKE	AAAIRDE	LQAFR**M**NGSGA		
α_3D-ChC1	MGSWAEFKQR	IAA**H**KTR	**C**QAL	GGS	H14, C18, H31
	EAELAA**H**EKE	IAAFESE	LQAF	KGKG	
	NPEVEALRKE	AAAIRDE	LQAFRLNGSGA		
α_3D-ChC2	MGSWAEFKQR	IAA**C**KTR	**H**QAL	GGS	C14, H18, H31
	EAELAA**H**EKE	IAAFESE	LQAF	KGKG	
	NPEVEALRKE	AAAIRDE	LQAFRLNGSGA		

[a]Bolded peptides were characterized in this work. Residues that are bolded in the sequence indicate metal binding residues. α_3D constructs were extended by four residues: GSGA.

interactions and manifests into a well-defined fold. *De novo* protein design offers a methodology in modeling the active sites of native proteins in a simplified or unrelated fold. DeGrado and co-workers made a significant advancement in protein design with their creation of a native-like scaffold, α_3D.[13] In contrast to previous *de novo* α-helical designs, α_3D is a single polypeptide chain of 73 amino acids that folds into an antiparallel three-helix bundle and contains every natural amino acid residue except cysteine (Table 1). We recently functionalized the α_3D scaffold with a metal binding site to produce α_3D**IV**[14] and α_3D**H$_3$**.[15] The first derivative, α_3D**IV**, contains a 3Cys site found in native CuT1 proteins to investigate the metallobiochemistry of toxic heavy metals,[14] and the NMR structure of apo α_3D**IV** was subsequently solved to investigate the perturbation on the overall fold of α_3D as a consequence of incorporating a 3Cys site in place of 3Leu residues.[16] The second derivative, α_3D**H$_3$**, possesses a 3His site that coordinates transition metal ions and was shown to recapitulate the catalytic reaction performed by carbonic anhydrase.[15]

In this work, we report the design process and characterization of copper metallopeptides that makes available a mixed first coordination sphere environment by modeling the 2HisCys(Met) metal binding site of native CuT1 proteins (Figure 1) within the α_3D scaffold. The preassembled fold of α_3D offers facile incorporation of a mixed-ligand site within a *de novo* designed scaffold. Utilizing the structure of α_3D**IV**[16] as a foundation, we designed three distinct constructs, designated as α_3D-core (CR), -chelate (CH), and -chelate-core (ChC) (Table 1). Our goal was to assess if the physical properties (e.g., absorption λ_{max} at 600 nm, compressed $A_{\|}$, short Cu–S(Cys) bond, and E° value >180 mV) of a metal center that is naturally observed in a β-barrel fold can be achieved in the antiparallel three-helix bundle fold of α_3D. Ultimately, the lessons learned from this work will provide the foundation to study long-rate ET reactions within a *de novo* designed

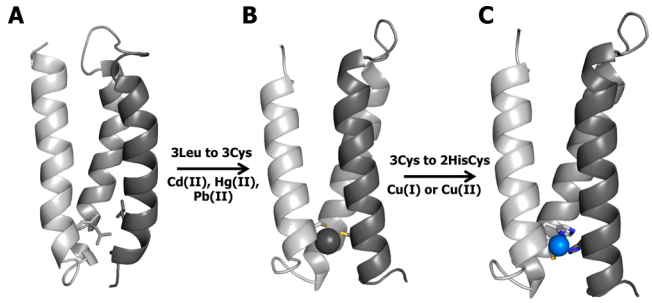

Figure 1. *De novo* design of α_3D constructs from a heavy metal binding site to a transition metal center. (A) Structure of α_3D (PDB 2A3D).[13] (B) Addition of 3Cys residues to the α_3D construct, producing α_3D**IV** with a modeled mercury atom (apo α_3D**IV** PDB 2MTQ).[16] (C) Redesign of α_3D**IV** to incorporate the core 2HisCys residues in native CuT1 proteins.

DOI: 10.1021/acs.inorgchem.5b01330
Inorg. Chem. 2015, 54, 9470–9482

framework and develop bifunctional/bimetallic constructs that contain a catalytic and an ET center, such as in copper nitrite reductase.

EXPERIMENTAL SECTION

Peptide Expression and Purification. A pET15B recombinant DNA plasmid that contains the gene for each construct was transformed and expressed in *E. coli* BL21(DE3) competent cells (Life Technologies). The plasmid for constructs α_3D-CR1, α_3D-CH3, α_3D-CH4, and α_3D-ChC2 (Table 1) were purchased from Celtek Genes. The Ala77Cys derivative of each construct was prepared for electrochemical studies. A GeneArt site-directed mutagenesis system (Life Technologies) was used to mutate the codon for Ala77 to Cys within the pET15b vector. These proteins were overexpressed in self-inducing media for 18 h, pelleted, resuspended in 1.0 mM phosphate buffer saline solution containing 2.0 mM dithiothreitol, and lysed by sonication. Protein purifications were performed using previously described methods.[16] These α_3D derivatives with a GSGA tail have a yield of 100−200 mg/L, which improved expression yields by 2 to 4 times compared to α_3D**IV**. The molecular weight is determined by ESI-MS (collected on a Micromass LCT time-of-flight mass spectrometer), which corresponds to the protein after the deletion of the N-terminal methionine residue. Protein concentrations were determined by measuring the absorbance at 280 nm using a determined ε = 5650 cm^{-1} M^{-1} (Trp) or 8215 cm^{-1} M^{-1} (Trp and Tyr).

Circular Dichroism (CD) Spectroscopy. CD spectra were collected on an AVIV 202 CD spectrometer at 25 °C using 1 cm path length quartz cuvettes. Samples contained 10 mM phosphate buffer and 5 μM peptide and were prepared at pH 7.5. The mean residue ellipticities ($[\theta]$) and percent folding were based on the presence of 55 helical residues, which were determined from the structure of α_3D**IV**[16] and were calculated using previously reported procedures.[17,18] Guanidine hydrochloride (GuaHCl) titrations were performed using a Microlab 500 series syringe-pump automatic titrator controlled by Aviv software. In a solution of 5 μM peptide in 10 mM phosphate buffer at pH 7.5, GuaHCl was titrated to a concentration of 5.0 M while maintaining the protein concentration. The change in molar ellipticity upon titration was fitted to a two-state unfolding model.[19]

Ultraviolet−Visible (UV−Vis) and Electron Paramagnetic Resonance (EPR) Spectroscopy. UV−vis spectra were recorded at room temperature on a Cary 100 Bio UV−vis spectrometer, using 1 cm path length anaerobic quartz cuvettes. X-band EPR spectra were collected on a Bruker EMX electron spin resonance spectrometer with a Varian liquid nitrogen cryostat at 77 K. A stock solution of standardized copper chloride was the source of Cu(II) ions. For the UV−vis experiments, 50 μM Cu(II) was added to a 100 μM apopeptide solution that contained 50 mM HEPES buffer solution. The pH of the apo solution was adjusted to 7.5. The spectrum was scanned from 800 to 300 nm every 2 min. EPR samples comprised 1 mM Cu(II)-peptide complex (at 1:2 Cu(II):peptide ratio), 50 mM HEPES solution, and 30% glycerol. Each sample was then flash frozen in liquid N_2. To obtain Cu(II) EPR parameters, each spectrum was simulated on SpinCount.[20]

^{113}Cd NMR Experiments. ^{113}Cadium(II) NMR experiments were performed on a Varian VNMRS 700 MHz equipped with a room-temperature triple resonance switchable probe and were collected at 25 °C. The reported chemical shifts are relative to the corresponding value of $Cd(ClO_4)_2$, 642 ppm, which is used as a zero point. The NMR parameters involved a spectral width of 96 000 Hz, 5.0 μs 90° pulse, and 0.05 s acquisition time with no delay between scans. Each sample was prepared by adding a small aliquot of $^{113}Cd(NO_3)_2$ (95% isotopically enriched ^{113}CdO purchased from Oak Ridge National Lab) to an apopeptide solution containing 15% D_2O/H_2O. The final solution yielded a ∼1 mM ^{113}Cd-peptide (with 20% excess peptide) complex, and the pH was adjusted to 8.5 with concentrated KOH. The ^{113}Cd NMR spectra were processed with MestreNova (version 10.0.0−14381) using a back linear prediction method.

Determination of Cu(I) Dissociation Constants. The Cu(I)-peptide dissociation constants were determined using a competitive binding assay with disodium bathocuproindisulfonate (BCS) as the competitive chelator, expressed by the chemical equation: Cu(I)Pep + 2BCS ⇄ $Cu(I)BCS_2$ + Pep. Each sample contained 25 μM Cu(I)-pep (at a 1:2 ratio of Cu:pep) and 50 mM HEPES buffer set to pH 7.5. A small aliquot of BCS was titrated into a sample solution and stirred for 12 min. The titration experiments were completed in triplicates. The formation of $CuBCS_2$ was tracked at 483 nm (ε = 13 300 cm^{-1} M^{-1}), which has a log β_2 of 19.8.[21] The binding constants were determined by fitting Abs vs BCS concentration plots on Hyperquad 2006 to the equation expressed above.

XAS Analysis. Samples for X-ray absorption spectroscopy (XAS) contained 1.0−2.0 mM Cu(I)-peptide complex, 50 mM buffer, and 30% glycerol in a glovebox. Samples were loaded into lucite XAS sample cells, frozen by immersion in liquid N_2, and stored at this temperature until data collection. Data were collected at the Stanford Synchrotron Radiation Lightsource (SSRL) on beamline 7-3 with a Si(220) double-crystal monochromator and a Rh-coated harmonic rejection mirror upstream of the monochromator with a 12 keV energy cutoff to reject harmonics. Data were measured in fluorescence mode using a high-count-rate Canberra 30-element Ge array detector, with maximum count rates held below 120 kHz per channel. A Ni filter was placed in front of the detector to reduce the elastic scatter peak, and Soller slits were used to reduce the Ni fluorescence. An Oxford Instruments liquid helium cryostat was used to keep the samples below 10 K during data collection. Data were collected using 10 eV steps in the pre-edge region (8700−8950 eV), 0.25 eV for the edge (8950−9010 eV) region, and k = 0.05 $Å^{-1}$ increments for the extended X-ray absorption fine structure (EXAFS) region to k = 13.5 $Å^{-1}$. These collections had integration times of 1 s in the pre-edge and edge regions and 1−20 s (k^3 weighted) in the EXAFS region for a total scan time of ∼40 min. Energies were calibrated by assigning the lowest energy inflection point of a copper metal foil as 8980.3 eV, placed between the second (I_1) and third (I_2) ionization chamber. An initial E_0 value of 8990 eV was used to convert data to k space, and the background was removed using a three-region cubic spline. Data from each detector channel were inspected for glitches before inclusion in the final average. For the XANES pre-edge, subtraction and normalization to McMaster[22] values were carried out using the program MBACK.[23]

Raw data were converted to EXAFS and fitted using the EXAFSPAK[24] suite of programs, with theoretical amplitude and phase parameters calculated using FEFF 9.[25] Each complex was fitted with four models: model 1, three-atom 1S2N(His) fit; model 2, four-atom 2S2N(His) fit; model 3, four-atom SS′2N(His) fit; and model 4, four-atom 1S1O2N(His) fit (Supporting Information, Table 2). Imidazole outer-shell scattering from the His was modeled using phase and amplitude parameters calculated for an idealized rigid $Cu(imid)_4$ structure. The imidazole Debye−Waller factors were defined by assuming that the σ^2 value for each scattering path increased proportionally from those calculated by Bunker and Dimakis for an ordered imidazole.[26] Two metal−ligand distances (R_{Cu-S}, R_{Cu-N}) and the Debye−Waller factors for the Cu−S and Cu−N shells (σ^2_{Cu-S}, σ^2_{Cu-N}) were the only adjustable parameters for models 1−3; for model 4 R_{Cu-O} and σ^2_{Cu-O} were also varied. The threshold energy E_0 was fixed at 0 eV for all fits.

Electrochemistry. Cyclic voltammetry measurements were obtained on a Metrohm AUTOLAB potentiostat (PGSTAT 12). The electrochemical apparatus contained a gold (Au) disk working electrode (0.008 cm^2), a platinum wire counter electrode, and an aqueous saturated calomel electrode (SCE) as the reference electrode (0.241 V + SCE = normal hydrogen electrode). The gold surface was polished with aqueous alumina slurries having decreasing particle sizes in the following order: 1−0.3−0.05 μm. Subsequently, the Au electrodes were conditioned in an electrochemical cell (under Ar_g), which contained 0.5 M H_2SO_4, by scanning 20 times from −300 mV to +1500 mV (vs SCE) at 500 mV/s until the cyclic voltammograms (CVs) overlaid well to indicate a homogeneous surface. The working electrode was also conditioned in the experiment cell, which

DOI: 10.1021/acs.inorgchem.5b01330
Inorg. Chem. 2015, 54, 9470−9482

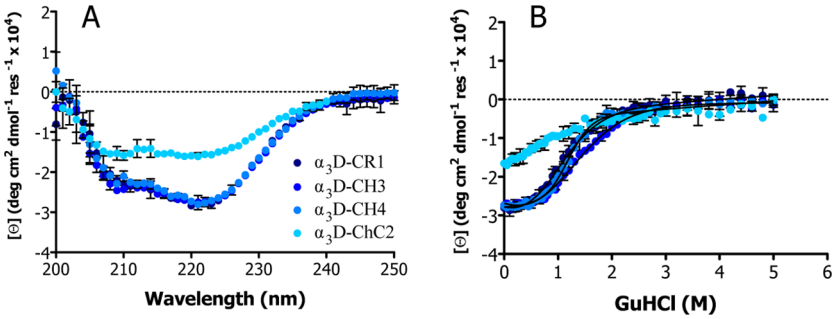

Figure 2. Circular dichroism spectra and chemical denaturation plots of apo α_3D-CR1, α_3D-CH3, α_3D-CH4, and α_3D-ChC2. (A) The CD spectra display two negative bands at 222 and 208 nm, demonstrating an α-helical structure. (B) Guanidine hydrochloride denaturations were fit to a two-state unfolding model.

comprised 0.1 M phosphate buffer and 0.1 M Na_2SO_4, scanning 10 times from −300 mV to +600 mV at 50 and 100 mV/s. After each electrode had been polished and conditioned, 20−50 μL of a 0.5 mM Cu(I)-peptide Ala77Cys solution was chemically adsorbed on the Au surface in an anaerobic environment for 1−2 h. CVs were collected at varying scan rates and at room temperature (~22 °C). Additional cyclic voltammetry experiments were performed on a BASi Epsilon potentiostat. A platinum wire counter, working Au (0.0201 cm^2), and Ag/AgCl (3.0 M NaCl) (0.210 V + Ag/AgCl = NHE) reference electrode were used in this experiment. This Au electrode was polished and conditioned, and the CVs were obtained using a similar procedure to that described above.

RESULTS

Solution Stability of Designed Constructs. The CD spectra of the apoform of α_3D-CR1, α_3D-CH3, α_3D-CH4, and α_3D-ChC2 (at pH 7.5) were collected to examine the perturbation of the overall fold of α_3D caused by the incorporation of 2HisCys residues. This analysis, as well as denaturation experiments, was not performed for α_3D-CH1, α_3D-CH2, and α_3D-ChC1 (*vide infra*). As shown in Figure 2A, each CD spectrum displays double minima bands with large negative molar ellipticity values [Θ] at 208 and 222 nm, illustrating a CD profile of a relatively well-folded α-helical scaffold.[27] The [Θ] indicated that α_3D-CR1, α_3D-CH3, and α_3D-CH4 are ~80% α-helical at pH 7.5. The same analysis performed on α_3D-ChC2, which buries the 2HisCys ligands deeper inside the bundle, revealed a protein that is ~35% less α-helical. The helicity of α_3D-ChC2 is reminiscent of the BABY[28] three-stranded coiled-coil peptide that has a similar helical length to α_3D. Guanidine hydrochloride titration experiments (Figure 2B) were performed to determine the Gibbs free energy of unfolding (ΔG_u), degree of cooperativity (m), and midpoint of the transition (C_m). These values were derived from a fit to a two-state unfolding model (Table 2). The m and C_m values have a range of 1.0−3.0 kcal mol^{-1} M^{-1} and 0.8−1.0 M, respectively. The ΔG_u parameter spans from 1.0 to 3.0 kcal mol^{-1}, with α_3D-CH4 demonstrating the highest value (3.2 kcal mol^{-1}). α_3D-ChC2 generated a broad denaturation shape, which indicated unfolding through several intermediate states, and the fit did not produce reliable denaturation parameters. Moreover, the corresponding experiments were performed on the Cu(I) adducts of each peptide to determine if metal binding improves stability. With the exception of Cu(I)α_3D-CH3, which showed a ~ 15% decrease, Cu(I) binding did not affect the α-helicity of these α_3D derivatives. Excluding α_3D-ChC2, the CD results showed that the apoforms have a high α-helical content, which was the goal of α_3D. Metal binding to the C-terminal end of the bundle (of

Table 2. Circular Dichroism Parameters

sample	% α-helicity[a]	m[b] (kcal mol^{-1} M^{-1})	C_m (M)[b]	ΔG_u[b] (kcal mol^{-1})
α_3D-CR1	79(3)	1.6(0.5)	0.8(0.1)	1.4(0.6)
α_3D-CH3	79(0)	1.2(0.1)	1.0(0.1)	1.3(0.1)
α_3D-CH4	80(2)	2.7(0.1)	1.2(0.0)	3.2(0.1)
α_3D-ChC2	45(1)			
Cu(I)α_3D-CR1	77(1)	1.3(0.1)	1.0(0.2)	1.2(0.2)
Cu(I)α_3D-CH3	61(3)	1.5(0.1)	1.3(0.1)	2.0(0.3)
Cu(I)α_3D-CH4	82(5)	2.1(0.0)	1.1(0.0)	2.4(0.0)
Cu(I)α_3D-ChC2	43(4)	1.6(0.2)	0.7(0.2)	1.1(0.4)

[a]Based on the presence of 55 helical residues, obtained from the structure of α_3D**IV**. [b]Derived from a two-step unfolding model. CD parameters were determined from duplicate experiments with pH values set to 7.5, and values in parentheses represent standard deviation.

α_3D-CR1, α_3D-CH3, and α_3D-CH4) was not expected to necessarily increase the helicity of the peptide because the overall fold is intrinsically highly helical. It is expected that metal binding could perturb the environment around the metal binding site of the peptide. The ΔG_u of Cu(I)α_3D-CH3 increased by 0.7 kcal mol^{-1}, while the corresponding parameter for Cu(I)α_3D-CH4 decreased by 0.8 kcal mol^{-1} compared to its apo counterpart. These results could be ascertained by the position of its Cys residue compared to α_3D-CH3. α_3D-CH4 has a Cys residue at the 18th position, whereas α_3D-CH3 contains the equivalent residue at position 21. The denaturation result of apo α_3D-CH4 suggests that the permutation of the Cys residue to the 18th from the 21st position and *vice versa* for the His residue (18th to the 21st) improves the overall fold of the α_3D-chelate construct by removing a bulky His and replacing it with a smaller Cys residue. Cu(I) binding to α_3D-CH4 perturbs the environment near its metal binding site, lowering its stability, whereas Cu(I) bound to α_3D-CH3 improves its stability at the cost of losing helicity. Additionally, Cu(I) binding to α_3D-CR1 did not have a significant effect on its stability, whereas the fit on the denaturation curve of Cu(I)α_3D-ChC2 generated CD parameters, indicating improvement on its stability when coordinated to Cu(I). The CD spectra and denaturation plots of the Cu(I) adducts are found in Supporting Information, Figure 1.

Characterization of Cu(II) Complexes. UV−vis spectra were collected for the Cu(II) complex of α_3D-CR1, α_3D-CH3,

DOI: 10.1021/acs.inorgchem.5b01330
Inorg. Chem. 2015, 54, 9470−9482

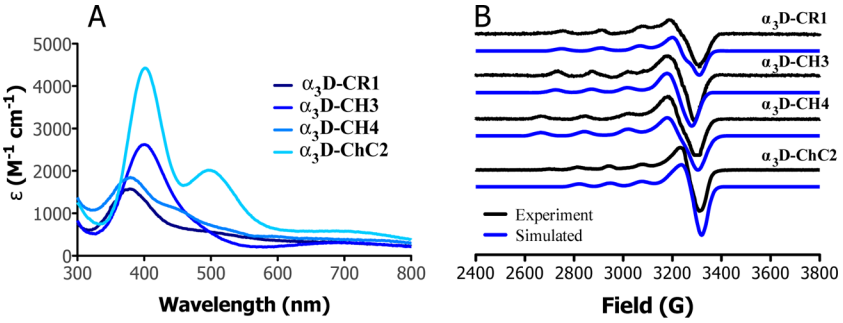

Figure 3. Overlay of Cu(II) UV−vis (A) and EPR (B) of designed constructs. (A) UV−vis spectra show a S(Cys) to Cu(II) LMCT band between 375 and 400 nm. These samples contained 100 μM peptide, 50 μM Cu(II), and 50 mM HEPES, with pH adjusted to 7.5. (B) EPR results display EPR spectra of axial Cu(II) species. These samples comprised a 1.0 mM Cu(II):peptide ratio (1 mM Cu(II):2 mM peptide) and 50 mM HEPES with pH set to 7.5, as well as 30% glycerol.

Table 3. Physical Properties of Designed Constructs

	λ nm (ε_λ M^{-1} cm^{-1})	$A_\parallel$ ($\times 10^{-4}$ cm^{-1}) g_x, g_y, g_z	K_d[a]		E^{0a} (mV vs NHE)
protein	Cu(II) complex		Cu(I) (fM)	Cu(II) (pM)	Cu(II/I)
α_3D-CR1	380(1565), 550(438), 600−800(300)	163	0.39(0.23)	0.1[b]	+398(23)[c,d]
	$R_{\varepsilon 380/550}$ = 3.6	2.05, 2.05, 2.21	0.06(0.02)[b]		+336[b,d]
α_3D-CH3	400(2619), 600−800(300)	152	3.04(0.68)	8.9	+364(19)[d]
	$R_{\varepsilon 400/550}$ = 11.9	2.04, 2.04, 2.24			
α_3D-CH4	377(1840), 450(1098), 520(600), 600−700(380)	185	11.13(2.07)	130	+399(3)[d]
	$R_{\varepsilon 377/540}$ = 3.3	2.04, 2.04, 2.25			
α_3D-ChC2	401(4429), 499(2020), 600−800(550)	130	10.48(3.21)	1400	+462(14)[e]
	$R_{\varepsilon 401/499}$ = 2.2	2.03, 2.03, 2.21			

[a]Values in parentheses represent the standard deviation. [b]pH 8.5. [c]pH 8.0. [d]Rate 1 mV/s. [e]Rate 10 mV/s. Cu(II) binding constants were derived from a Nernst equation analysis on the reduction potential and Cu(I) binding constants. pH set to 7.5.

α_3D-CH4, and α_3D-ChC2 (Figure 3A). These results are summarized in Table 3 and compared to the corresponding properties of native and mutant CuT1 proteins, as well as CuT1 models in Supporting Information, Table 1. Cu(II)α_3D-CR1 displayed a CuT2 species with an LMCT absorption band at 380 nm (1565 M^{-1} cm^{-1}), a shoulder at 550 nm (438 M^{-1} cm^{-1}), and a broad d−d-like band between 600 and 800 nm (300 M^{-1} cm^{-1}). Cu(II)α_3D-CH3 formed a yellow copper species with an intense band at 400 nm (2619 M^{-1} cm^{-1}) and a broad band between 600 and 800 nm (300 M^{-1} cm^{-1}). Similarly, the Cu(II) adduct of α_3D-CH4 showed a λ_{max} at 377 nm (1840 M^{-1} cm^{-1}). This complex, however, has additional red-shifted bands at 450 (1098 M^{-1} cm^{-1}) and 520 (600 M^{-1} cm^{-1}) nm. Cu(II)α_3D-ChC2 exhibited two distinct intense LMCT bands at 401 nm (4429 M^{-1} cm^{-1}) and 499 (2020 M^{-1} cm^{-1}). This complex formed a brown-orange copper species in solution (Supporting Information, Figure 2), which has been previously observed in the Met to Glu mutant of azurin[29] and rusticyanin.[30] The R_ε value is widely used to categorize native and designed CuT1 centers and determined from the ratio of the molar extinction coefficient at ∼400 (±50) and ∼600 (±50) nm. This value signifies the deviation from a trigonal pyramidal to a tetrahedral or tetragonal/square planar geometry: blue and green copper centers have an R_ε value less than 0.1 (trigonal pyramidal) and 0.1−0.6 (pseudotetrahedral), respectively, while CuT2 centers such as nitrosocyanin have a ratio greater than 1.0 (tetragonal). The Cu(II) adducts of α_3D-CR1, α_3D-CH3, α_3D-CH4, and α_3D-ChC2 have R_ε values of 3.6, 11.9, 3.3, and 2.2, respectively. The R_ε values for the designed constructs were derived from their λ_{max} (377−400 nm) and a second band between 500 and 550 nm. Moreover, upon the addition of Cu(II), the absorption features of each complex faded with varying times. This bleaching effect is due to a redox reaction between the copper and S(Cys) ligand, which reduces the Cu(II) ion.[31,32] The spectrum of Cu(II)α_3D-CR1 and Cu(II)α_3D-CH4 bleached after 10 min, while the Cu(II)α_3D-CH3 species slowly faded over a 4 h time span, demonstrating a more stable Cu(II)−S(Cys) bond. The spectrum of Cu(II)α_3D-ChC2 persisted for ∼15 h, exhibiting the most stable Cu(II)−S(Cys) bond of the designed constructs (Supporting Information, Figure 3). The Cu(II) spectra of α_3D-CH1, α_3D-CH2, and α_3D-ChC1 were completely autoreduced in 5 min; therefore these constructs were not characterized further. Moreover, a copper EPR spectrum was collected for each construct (Figure 3B). The EPR parameters from the simulation are listed in Table 3. Each complex displayed an axial EPR spectrum and $g_\parallel > g_\perp > 2.0023$, which signifies a Cu(II) $3d_{x^2-y^2}$ ground state. Cu(II)α_3D-CR1, Cu(II)α_3D-CH3, and Cu(II)α_3D-CH4 have $A_\parallel$ values that range from 150 to 190 × 10^{-4} cm^{-1}. Cu(II)α_3D-ChC2 has the respective value of 130 × 10^{-4} cm^{-1}.

Comparative Metal Binding Study Using ^{113}Cd NMR. To evaluate metal binding to the 2HisCys(Met) sites further, ^{113}Cd NMR spectra were collected for α_3D-CR1, α_3D-CH3, and α_3D-ChC2 (Supporting Information, Figure 4). The ^{113}Cd nucleus is highly sensitive to its ligand field environment and has been used to probe the binding site of native metalloproteins.[33,34] The ^{113}Cd NMR spectrum of α_3D-CR1 displayed two resonance signals, a sharp and broad signal, at 320 and 363 ppm, while ^{113}Cdα_3D-CH3 showed one resonance signal at 342 ppm. ^{113}Cd(II)α_3D-ChC2 exhibited a single resonance at 336 ppm. These results revealed that α_3D-CR1 formed two Cd(II) conformations, whereas α_3D-CH3 and α_3D-

DOI: 10.1021/acs.inorgchem.5b01330
Inorg. Chem. 2015, 54, 9470−9482

ChC2 both produced a single species. The species with a chemical shift between 320 and 340 ppm suggest a Cd(II) ion bound to at least an N_2S ligand set, while values at 360 ppm could indicate an addition of an S(Met) (S*) and/or an O atom (from a water molecule or the peptide) ligand(s), representing a $N_2SS^*O_x$ environment.[34] This ^{113}Cd chemical shift value is only 10−20 ppm upfield from azurin and stellacyanin. These chemical shift values are compared to cadmium-substituted native cupredoxins in Table 4.

Table 4. ^{113}Cd NMR Chemical Shift Comparison to Native Proteins

^{113}Cd-protein	chemical shift (ppm)	donor set
carbonic anhydrase	210−270	N_3O
α_3D-ChC2	336	N_2SO_n[a]
α_3D-CR1	320 and 363	N_2SO_n[a] or N_2SS^*[a]
α_3D-CH3	342	N_2SO_n[a]
Pseudomonas azurin	372	N_2SS^*
Alcaligenes azurin	379	N_2SS^*
stellacyanin	380	N_2SS^*O
Spinacea plastocyanin	432	N_2SS^*
alcohol dehydrogenase	483	N_2S_2

[a]Predicted donor set for designed constructs.

Determination of Cu(I) and Cu(II) Dissociation Constants. The Cu(I) dissociation constants (K_d) at pH 7.5 of α_3D-CR1, α_3D-CH3, α_3D-CH4, and α_3D-ChC2 were determined from a competition assay that utilized the chelating agent BCS ($CuBCS_2$: log β_2 = 19.8 and $\varepsilon_{483\ nm}$ = 13 300 cm^{-1} M^{-1}).[21] The spectra and titration curves for this work are found in Supporting Information Figure 5. This competition study produced K_d values of 0.4−11 fM (Table 3). Constructs α_3D-CH4 and α_3D-ChC2 have the highest K_d values of 11.3(2.07) and 10.48(3.21) fM, respectively. α_3D-CH3 has a K_d value of 3.04(0.68) fM. α_3D-CR1 formed the strongest complex and has K_d values of 0.39(0.23) and 0.06(0.02) fM at pH 7.5 and 8.5, respectively.

Moreover, Cu(II) binding constants were calculated from the Nernst equation: $E^0_{Pep} = E^0_{Cu(II/I)} + 0.0591 \log(K_d^{Cu(II)}/K_d^{Cu(I)})$, where E^0 is the reduction potential for the peptide construct and E^0Cu(II/I) is the potential for the couple Cu(II/I) (0.159 V vs NHE). The derived Cu(II) binding constants for α_3D-CR1 and α_3D-CH3 are 60 and 8900 fM, respectively, while α_3D-CH4 and α_3D-ChC2 have a much weaker affinity for Cu(II) of 1.3×10^5 and 1.4×10^7 fM, respectively. Overall, the designed constructs bind copper with 1 to 5 orders of magnitude weaker affinity than azurin, which has corresponding values of 0.03 and 25 fM for Cu(I) and Cu(II) at pH 7.0.[35]

X-ray Absorption Analysis on Cu(I) Complexes. To assess copper binding to the designed metal binding sites further, the Cu(I) complexes of α_3D-CR1, α_3D-CH3, α_3D-CH4, and α_3D-ChC2 were analyzed by XAS. The X-ray absorption near edge structure (XANES) spectra (Figure 4) are consistent with those typically observed for a Cu(I) complex, exhibiting a Cu(I) pre-edge peak at ∼8984 eV that is attributed to a 1s → 4p transition.[36] The relatively intense transition for Cu(I)α_3D-CR1 and Cu(I)α_3D-ChC2 is consistent with a three-coordinate species,[37] while the lower intensity pre-edge feature for Cu(I)α_3D-CH3 and Cu(I)α_3D-CH4 suggests a four-coordinate geometry.

Subsequently, EXAFS was used to obtain metrical parameters on the Cu(I) species (Table 5). The Fourier transforms (FT)

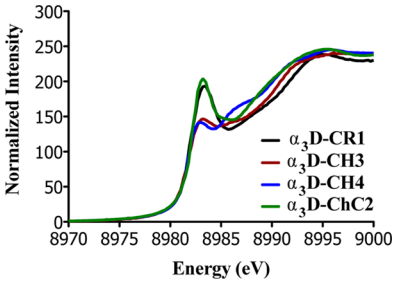

Figure 4. Comparison of the XANES plot of Cu(I)α_3D-CR1, Cu(I)α_3D-CH3, Cu(I)α_3D-CH4, and Cu(I)α_3D-ChC2. In each plot, a resolved peak at ∼8984 eV is observed that is attributed to a Cu(I) 1s → 4p transition.[36]

Table 5. EXAFS Fitting Parameters[a] of Cu(I) Complexes

		Cu−S		Cu−N		
sample	model	R (Å)	σ^2 (Å^2)	R (Å)	σ^2 (Å^2)	F
α_3D-CR1	1	2.16	0.0034	1.92	0.0091	112
α_3D-CH3	2	2.20	0.0031	1.95	0.0074	143
α_3D-CH4	2	2.23	0.0039	1.99	0.0137	70
α_3D-ChC2	1	2.18	0.0042	1.92	0.0154	68
P. Aeruginosa azurin[38]		2.21	0.0031	2.00	0.0040	
C. Sativus stellacyanin[39]		2.22	0.0016	2.02	0.0015	
N. europea nitrosocyanin[40]		2.28	0.0005	1.96	0.0004	

[a]Model (number of scatters), R (distance), σ^2 (Debye−Waller factor), F (goodness of fit). Samples were prepared at pH 7.5. Ref 38 pH 5.5. Ref 39 pH 5.5. Ref 40 pH 7.0.

of the EXAFS data for all four samples are dominated by a single intense peak at $R \approx 2$ Å (Figure 5), indicating the presence of a heavy scatterer such as a sulfur atom. In addition, the FTs also show weak outer-shell scattering consistent with multiple scattering from a His residue. The lack of a resolvable Cu−N peak in the FT reflects the low scattering power of N in comparison with S. Each spectrum was fitted to four models: CuN_2S (model 1), CuN_2S_2 (model 2), CuN_2SS^* (model 3), and CuN_2SO (model 4). The Cu(I) adducts could be fit to a Cu−S and Cu−N scattering environment at ∼2.2 and ∼2.0 Å, respectively. The fitted Cu-nearest-neighbor distances vary as expected, given the apparent coordination numbers of 3 for Cu(I)α_3D-CR1 and Cu(I)α_3D-ChC2 and 4 for Cu(I)α_3D-CH3 and Cu(I)α_3D-CH4. The three-coordinate fits produced Cu−S(Cys) and Cu−2N(His) bond lengths of 2.16−2.18 and 1.92 Å, respectively. The four-coordinate fits yielded Cu−2S and Cu−2N(His) distances of 2.20−2.23 and 1.95−1.99 Å, respectively. Although some of the samples could be fit with a third shell of scatters (either Cu−S or Cu−O) these models did not improve the fit quality and resulted in chemically unlikely distances and Debye−Waller factors (σ^2) (Supporting Information, Table 2). For instance, the best fits for Cu(I)α_3D-CH3 and Cu(I)α_3D-CH4 were obtained with a shell of two S atoms and a Debye−Waller factor of (3−4) × 10^{-3} Å^2. In contrast, attempts to fit these data with only a single S atom resulted in higher F values and small Debye−Waller factors (∼2 × 10^{-4} Å^2). The opposite trend was observed for Cu(I)α_3D-CR1 and Cu(I)α_3D-ChC2. The best fits were obtained using a single Cu−S, and these fits produced reasonable Debye−Waller factors of (3−4) × 10^{-3} Å^2. Overall, the EXAFS analysis is consistent with the change in coordination number that is

DOI: 10.1021/acs.inorgchem.5b01330
Inorg. Chem. 2015, 54, 9470−9482

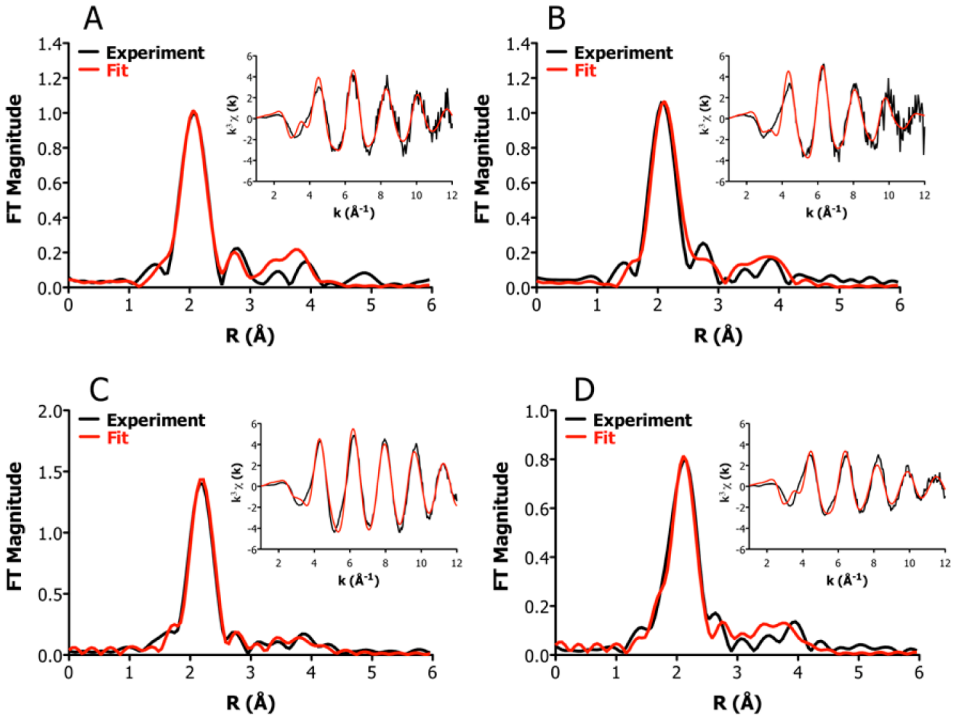

Figure 5. EXAFS (as inset) and Fourier transform plot of Cu(I)α_3D-CR1 (A), Cu(I)α_3D-ChC2 (B), Cu(I)α_3D-CH3 (C), and Cu(I)α_3D-CH4 (D). These plots represent the best model for each Cu(I) complex: a three-atom fit for Cu(I)α_3D-CR1 and Cu(I)α_3D-ChC2 and a four-atom fit for Cu(I)α_3D-CH3 and Cu(I)α_3D-CH4.

indicated by the XANES as a consequence of an additional S atom. The second S atom is predicted to originate from the S(Met72) ligand. Even though these distances are ~0.6 Å shorter than what is observed in the X-ray crystal structures of native cupredoxins, Cu(I)−thioether bonds of 2.20 Å have been measured in small-molecule compounds (Supporting Information, Table 3).

Cu(II/I) Reduction Potential of Designed Constructs. The reduction potential ($E°$) for the Cu(II/I) couple of α_3D-CR1 (pH 8.0 and 8.6), α_3D-CH3 (pH 7.5), α_3D-CH4 (pH 7.5), and α_3D-ChC2 (pH 7.5) was determined using protein film electrochemistry (Table 3).[41] The Cu(I) form of the Ala77Cys mutant of each construct was irreversibly adsorbed on a gold working electrode, and cyclic voltammograms were collected at varying scan rates. The grafted peptide formed a stable electroactive film, as demonstrated by Figure 6A. An overlay of apo and copper-bound peptide in Figure 6B shows that the copper center participates in an ET reaction with the Au surface. The cathodic and anodic peak separation (ΔE_p) ranges from 40 to 130 mV, values that have also been observed

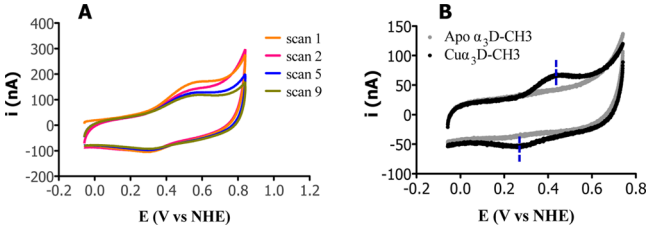

Figure 6. (A) Cyclic voltammograms of Cuα_3D-CR1 (pH 8.0) at 100 mV/s. (B) CV of apo α_3D-CH3 and Cuα_3D-CH3 (pH 7.5) at 100 mV/s. Electrochemical working cell contained 100 mM phosphate buffer and 100 mM sodium sulfate purged with Ar_g.

in adsorbed CuT1 proteins (Supporting Information, Table 4). Our observed ΔE_p values suggest very sluggish electron transfer between the surface and the copper center and/or poor orientation on the surface. The surface coverage of the adsorbed protein (Γ_T) was determined from 1 to 13 × 10^{-10} mol cm^{-2} (Supporting Information, Table 4) and was derived from *area of reduction peak*/ν = $nFA\Gamma_T$, where n is the number of electrons transferred, F is Faraday's constant (96 487 C mol^{-1} of electrons), A is electrode area in cm^2, Γ_T is the total surface concentration of electroactive protein, and ν is the scan rate (100 mV/s). The reduction potentials were determined from an analysis of peak potentials as a function of scan rate over a broad range (Supporting Information, Figure 8). The trumpet plots show that the ΔE_p decreases as the scan rate becomes smaller, and according to Laviron,[42] the two curves, anodic and cathodic, converge to the same asymptote, having $y = E^0$. The reduction potential (E^0) can be estimated as the average of the cathodic and the anodic peak potentials at the scan rate corresponding to the minimal peak split. α_3D-CR1, α_3D-CH3, and α_3D-CH4 have an E^0 range of +364 to +399 mV (vs NHE). α_3D-ChC2 displayed a higher potential of +462 mV. These values are within the range observed for plastocyanin (+404 mV) and azurin (+361 to +406) grafted on a Au surface (Supporting Information, Table 4).

DISCUSSION

After previously establishing that the α_3D scaffold can accommodate cysteine ligands bound to a heavy metal and bulky His ligands that can coordinate a transition metal, we then designed α_3D constructs that presented mixed-ligand environments such as the 2HisCys metal binding site of CuT1 centers (Figure 7). The preassembled fold of α_3D provides a more direct incorporation of a mixed-ligand/asymmetric metal center than many of the three-stranded coiled-coil constructs

DOI: 10.1021/acs.inorgchem.5b01330
Inorg. Chem. 2015, 54, 9470−9482

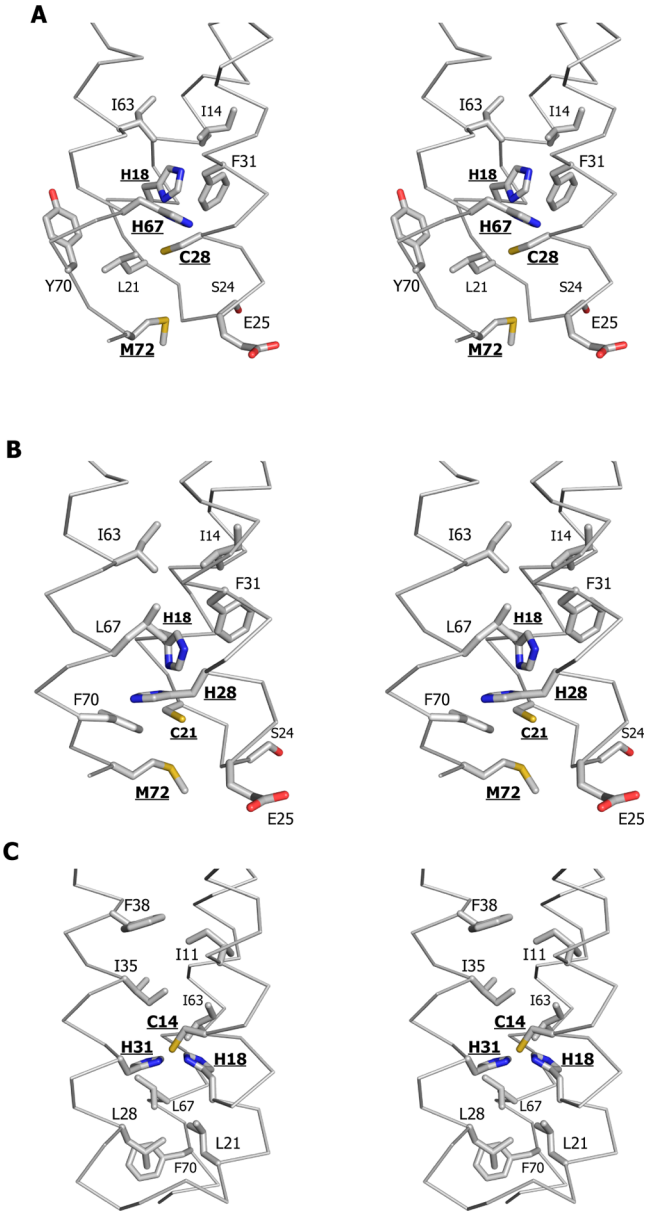

Figure 7. Stereodiagrams of designed constructs based on the α_3DIV[16] structure. The 2His, Cys, and/or Met ligands are bolded and underlined. Hydrophobic (I, L, F, and Y) residues and possible competing ligands S24 and E25 are also labeled. (A) Core construct α_3D-CR1 contains N_2SS^* ligands at the C-terminal end of the bundle, at positions 18, 67, 28, and 72. (B) Chelate construct α_3D-CH3 possesses a Cys−X−X−His chelating motif at the 18th and 21st position, respectively, as well as a second His ligand at the 28th and Met ligand at the 72nd position. These ligands are also located at the C-terminal end. (C) In α_3D-ChC2, a chelate-core construct, N_2S CuT1 ligands are translated one layer above toward the N-terminal end. This construct contains a C14−X−X−X−H18 chelating motif and a second His ligand at the 31st position, which are capped by apolar residues.

we have examined previously. Furthermore, this work allows us to investigate whether the unique spectroscopic, structural, and redox properties of native CuT1 proteins can be retained in an unrelated α-helical fold. This is particularly important for assessing the importance of the weakly coordinated carbonyl groups that are unavailable for metal binding within an α-helical structure.

α_3D-CR1 incorporates the 2HisCys residues on three separate strands, at positions 18, 28 and 67, and a Met residue at position 72 (Figure 7A). With the exception of Met72, this metal binding site mirrors the 3Cys positions in α_3DIV. The absorption spectrum of Cu(II)α_3D-CR1 exhibited the absorption features of the CuT2 site with a λ_{max} at 380 nm (1565 M^{-1} cm^{-1}) and broad d−d-like bands between 600 and 700 nm (300 M^{-1} cm^{-1}). The EPR hyperfine coupling constant of this complex is ~60 × 10^{-4} cm^{-1} greater and the R_ε value ($\varepsilon_{380\ nm}/\varepsilon_{550\ nm}$) is ~4 times higher than the corresponding parameters for green copper sites. On the basis of the characterization of nitrosocyanin[40,43] and a reengineered copper−zinc superoxide dismutase,[44,45] the absorption band that dominates much of the Cu(II) spectrum of α_3D-CR1 stems from an LMCT from the S(Cys)$\sigma \rightarrow$ Cu $d_{x^2-y^2}$ charge transfer transition that is expected for CuT2 centers with tetragonal geometry as a consequence of the Jahn−Teller effect.[7,43]

The design concept of the second constructs was inspired by the L−X_n−L (L= His or Cys, n = nonligating residues) chelate motif found in the loop regions of zinc finger proteins, as well as cupredoxins. The first CH derivative, α_3D-CH1, contains a His-X_2-His chelate group at the 18th and 21st positions and a Cys and Met at positions 28 and 72, respectively. The second iteration, α_3D-CH2, has a His18-X_3-Cys22 chelate group (via a Gly22Cys, Cys28His, and His67Leu mutation of α_3D-CR1), as well as a His28 and Met72 residue. The first two CH constructs were very unstable when bound to Cu(II) and were not characterized further. CH constructs α_3D-CH3 and α_3D-CH4 possess a Cys−X_2−His chelate motif at the end of helix 1, at positions 18 and 21, as well His 28 and Met 72 (Figure 7B). Compared to the CR construct, the chelate group was designed to provide a strong Cys−Cu−His bond and requires one additional helix to provide the second His ligand. The 21st position, which is the first residue in loop 1, was chosen because the apolar group of Leu 21 in the α_3DIV structure is oriented toward the N-terminal end of the bundle. Replacing Leu 21 with a Cys or His residue could provide an analogous rotamer. α_3D-CH3 has a His18−X_2−Cys21 chelate group, and α_3D-CH4 contains an inverted arrangement of this group (Cys18−X_2−His) and translates the Cys residue three positions toward the N-terminal end. In addition, Tyr45/70Phe substitutions were performed on both constructs to serve as a hydrophobic capping element, which could deter access by water molecules or competing ligands.

Even though both complexes generated spectra comparable to CuT2 centers, the absorption profiles of Cu(II)α_3D-CH3 and Cu(II)α_3D-CH4 are distinctive. The Cu(II)α_3D-CH3 complex formed a yellow tetragonal species, exhibiting an intense S(Cys)$\sigma \rightarrow$ Cu $d_{x^2-y^2}$ transition at 400 nm (2619 M^{-1} cm^{-1}) and a broad band between 600 and 800 nm (300 M^{-1} cm^{-1}), as well as an R_ε value of 11.9 ($\varepsilon_{400\ nm}/\varepsilon_{550\ nm}$). Cu(II)$\alpha_3$D-CH4 also displayed a λ_{max} toward the UV range at 377 nm (1840 M^{-1} cm^{-1}). However, the inverted chelate group of α_3D-CH4 exhibited additional absorption bands at 450 and 520 nm and an R_ε value ($\varepsilon_{400\ nm}/\varepsilon_{540\ nm}$) of 3.3, 4 times lower than that for α_3D-CH3. Moreover, this complex formed a green color at a high concentration, revealing the additional transitions in the visible range (Supporting Information, Figure 2). Unexpectedly, the $A_{||}$ value of Cu(II)α_3D-CH4 is ~30 × 10^{-4} cm^{-1} greater than the equivalent parameter of Cu(II)α_3D-CH3; yet both values are still within the range of CuT2 centers (>100 × 10^{-4} cm^{-1}).

DOI: 10.1021/acs.inorgchem.5b01330
Inorg. Chem. 2015, 54, 9470−9482

Overall, even though the Cu(II) complex of α_3D-CH3 and α_3D-CH4 displayed UV−vis spectra that are indicative of tetragonal CuT2 species, the Cys/His18−X_2−Cys/His21 chelate group has a noteworthy effect on Cu(II) binding. The additional bands in the spectrum of α_3D-CH4 could signify a weakening of the interaction between the S(Cys)σ and Cu $d_{x^2-y^2}$ orbital, perhaps as a consequence of placing the Cys residue closer to the hydrophobic core of the bundle. In terms of the α_3D-CH3 construct, the Cu(II) complex does not rapidly undergo an autoreduction reaction and can persevere for ∼4 h. This observation demonstrates that the chelate group in α_3D-CH3 is able to form a more stable Cu(II)−S(Cys) bond compared to α_3D-CR1 and α_3D-CH4.

The Cu(II) binding results revealed that the metal binding site of the core and chelate constructs was insufficient in forcing the Cu(II) to form an entatic state.[46,47] That is, the Cu(II) ion is dictating the coordination environment by forming its preferred tetragonal complex. To improve on these previous results, the third construct was designed to incorporate a chelate group within the core of the α_3D scaffold, with the intention of constraining the metal binding site through steric interactions. From NMR studies, DeGrado and co-workers observed that the aromatic groups of Trp4, Phe7, and Tyr45 forced the methyl groups of Leu42, Val53, and Leu56 into an ordered and less dynamic state.[48] To achieve more control, we encapsulated the metal binding site of α_3D-ChC1 and α_3D-ChC2 inside a hydrophobic box that could provide analogous steric pressure on the 2HisCys residues. The overall objective was to allow the protein environment to dictate the geometry of the copper complexes and deter the formation of a tetragonal species. The hydrophobic box comprises a plane formed by Leu21, Leu28, Leu67, and Phe70 at the C-terminal and Ile11, Ile35, Phe38, and Ile63 at the N-terminal end (Figure 7C). The first chelate-core construct, α_3D-ChC1, has a His14−X_3−Cys18 chelate group, and a second His at the 31st position, the Met ligand was removed. Due to its instability when bound to Cu(II), this construct was also not characterized further. α_3D-ChC2 possesses a Cys14−X_3−His18 chelate motif, as well as His 31, modeling the metal binding site of plantacyanin and the CuT1 site in laccase. In essence, α_3D-ChC2 contains the respective metal binding site of α_3D-CH4, translated one layer toward the N-terminal end of the bundle.

In contrast to the core and chelate constructs, Cu(II)α_3D-ChC2 displayed two intense CT bands at 401 (4429 M^{-1} cm^{-1}) and 499 (2020 M^{-1} cm^{-1}), producing a brown copper species with an R_ε ($\varepsilon_{401\ nm}/\varepsilon_{499\ nm}$) of 2.2. When compared to Cu(II)α_3D-CH4, the λ_{max} of Cu(II)α_3D-ChC2 is red-shifted by 24 nm, and the intensity of this band increased by 2 fold. The second band at 499 nm (at 520 nm in Cu(II)α_3D-CH4) is more defined and intense than the corresponding bands in the previous constructs. This Cu(II) complex is also the more long-lived (∼15 h), demonstrating a stable Cu(II)−S(Cys) bond (Supporting Information, Figure 3). The hyperfine coupling constant value of Cu(II)α_3D-ChC2 is 130 × 10^{-4} cm^{-1}, which is nevertheless ∼30 × 10^{-4} cm^{-1} greater than the $A_{||}$ values of its native counterparts. Moreover, the Cu(II) spectroscopic features of Cu(II)α_3D-ChC2 are comparable to the oxidized form of Met148Glu rusticyanin[30] and Met121Glu azurin,[49] which both displayed a brown copper species (at pH > 6) with a λ_{max} between 396 and 416 and a second less intense band at ∼570 nm, as well as $A_{||}$ values greater than 90 × 10^{-4} cm^{-1}. This comparison shows that the chelate-core design was able to recapitulate a mutated CuT1-like site within the α_3D fold and provides insight into future designs for chelate-core constructs to achieve a pure CuT1 site.

It is conceivable that there are competing ligands that are provided by the peptide or the solvent that lead to tetragonal Cu(II) complexes. In order to test this hypothesis, a comparative metal binding study using ^{113}Cd(II) NMR was performed on α_3D-CR1, α_3D-CH3, and α_3D-ChC2 (Supporting Information, Figure 4). ^{113}Cd(II) NMR provides a sensitive method to probe the coordination environment of metal centers[33] and could offer insight into Cu(II) binding in the designed constructs. The ^{113}Cd(II) NMR spectrum of α_3D-CR1 indicated the formation of competing species, which is represented by the two resonances at 320 and 363 ppm. Compared to the reported chemical shift values for native CuT1 proteins, the downfield resonance peak of ^{113}Cd(II)α_3D-CR1 is 9−16 and 17 ppm upfield from azurin (373−379 ppm) and stellacyanin (380 ppm),[33,34] respectively, demonstrating that the ∼360 ppm species share an equivalent donor set as their native counterparts. This comparison suggests that the S(Met) can serve as a fourth ligand, which is not evident in the Cu(II) binding studies. Moreover, the upfield species of ^{113}Cd(II)α_3D-CR1 is ∼100 ppm downfield of CdN_3O complexes (∼310−330 ppm) and instead implies an N_2SO_x donor set, where the O ligands could stem from exogenous $^-OH/H_2O$ molecules or the side chain of residues on the first loop of the bundle, such as Ser24 or Glu25. Moreover, the ^{113}Cd NMR spectrum of α_3D-CH3 and α_3D-ChC2 show single peaks at 342 and 336 ppm, respectively, signifying the presence of one cadmium species with an N_2S or N_2SO_x donor set.

One of the characteristic physical properties of native cupredoxins is their short Cu−S(Cys) bond. To determine if the designed constructs can reproduce the reduced form of CuT1 proteins, XAS analysis was performed on the Cu(I) adducts of α_3D-CR1, α_3D-CH3, α_3D-CH4, and α_3D-ChC2 (Table 5). The XANES spectra of Cu(I)α_3D-CR1 and Cu(I)α_3D-ChC2 overlay well, as do the spectra for Cu(I)-α_3D-CH3 and Cu(I)α_3D-CH4, suggesting that each set of Cu(I) complexes share a similar coordination environment. The first pair showed a XANES pre-edge feature indicative of a three-coordinate complex, whereas the latter pair have XANES spectra that are more consistent with a four-coordinate environment. These conclusions were supported with the EXAFS analysis. The Cu(I) adducts of α_3D-CR1 and α_3D-ChC2 fitted well to a three-atom environment that consists of an S atom and two N atoms. Cu(I)α_3D-CR1 has a Cu(I)−S(Cys) bond of 2.16 Å, while the corresponding bond in the chelate-core design of α_3D-ChC2 elongates slightly to 2.18 Å. The Cu(I)−2N(His) bonds in both complexes have an average Cu−N bond length of 1.92 Å. Since α_3D-ChC2 possesses a 2HisCys binding site, this construct should favor the formation of a three-coordinate Cu(I) complex; therefore, the Cu(I)α_3D-ChC2 complex can be viewed as a pseudointernal standard for validating the coordination number of Cu(I)α_3D-CR1. Therefore, their very similar XANES and the very similar Cu−ligand distance both point to Cu(I)α_3D-CR1 and Cu(I)α_3D-ChC2 having equivalent Cu(I)N_2S local structures.

A similar comparison of the Cu(I) complex of α_3D-CH3 and α_3D-CH4 can be established. Cu(I)α_3D-CH3 fitted well to a 2S-2N four-atom model (model 2). The Cu(I)−2S has a bond length of 2.20 Å and the Cu(I)−2N(His) has a bond distance of 1.95 Å, both somewhat longer than seen in the three-coordinate complexes. Cu(I)α_3D-CH4 is also fitted well to

DOI: 10.1021/acs.inorgchem.5b01330
Inorg. Chem. 2015, 54, 9470−9482

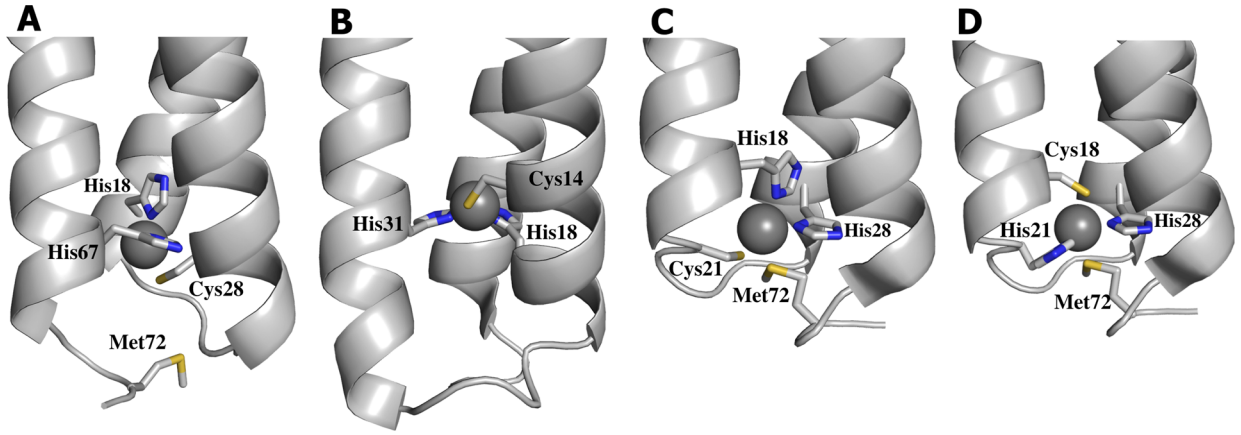

Figure 8. Models of the reduced state based on the EXAFS analysis of the designed constructs. (A) Cu(I)α_3D-CR1. (B) Cu(I)α_3D-ChC2. (C) Cu(I)α_3D-CH3. (D) Cu(I)α_3D-CH4. The chelate constructs are able to form a short Cu−S(Met) bond of ∼2.2 Å, which indicates that the copper ion is closer to loop 1 at the C-terminal end compared to the Cu(I) complex in α_3D-CR1.

model 2, with average Cu(I)−2S and Cu(I)−2N(His) distances of 2.23 and 1.99 Å, respectively. The second sulfur ligand in both complexes is likely to originate from S(Met72). While the Cu(I)−S(Met) bond in native CuT1 centers has a much longer bond length (2.6−2.9 Å),[5] a Cu(I)−SR_2 bond at ∼2.2 Å has been observed in the X-ray crystal structure of small-molecule compounds (see Supporting Information, Table 3). Thus, it is possible that such a short Cu(I)−S(Met) bond can form in α_3D-CH3 and α_3D-CH4 but not in native cupredoxins because the distance of the axial ligand from the copper center is controlled by aromatic side chains. The observation of S and His ligation implies that location of the metal binding site of α_3D-CH3 and α_3D-CH4 is arranged at the end of the bundle. As a consequence, the copper complex is at the interface of the C-terminal end and allows for the S(Met) ligand to form a short bond, as illustrated in Figure 8.

Native CuT1 centers have a uniquely short Cu−S(Cys) bond with an average distance range between ∼2.07 and 2.25 Å, in contrast to the more normal Cu−cysteine distances of 2.3−2.4 Å.[5,7] The bond lengths from the EXAFS analysis were compared to the corresponding derived values of native CuT1 proteins (Table 5). The bond lengths of the designed Cu(I) adducts are compared to the reduced state of a blue (*P. aeruginosa* azurin),[38] green (*C. sativus* stellacyanin),[39] and red (*N. europea* nitrosocyanin) copper center.[40] The EXAFS analysis on the Cu(I) adducts of the designed constructs exhibited metal centers with bond lengths and coordination numbers that are comparable to their native counterparts. The Cu(I)−S(Cys) bonds of Cu(I)α_3D-CR1 and Cu(I)α_3D-ChC2 deviate the most from the native examples, with bond lengths that are shorter by ∼0.04 Å. This is consistent with these two complexes having a three-coordinate environment. The four-coordinate model of Cu(I)α_3D-CH3 and Cu(I)α_3D-CH4 has a Cu(I)−S(Cys) bond that is virtually equivalent to the respective bond in azurin and stellacyanin but ∼0.05 Å shorter than that in nitrosocyanin. This comparison indicates that the coordination environment of Cu(I)α_3D-CH3 and Cu(I)α_3D-CH4 is more similar to a blue or green than a red copper center. By and large, the XAS analysis illustrates that the designed constructs were able to recapitulate the reduced form of CuT1 centers within the α_3D scaffold.

In addition to the signature spectroscopic and structural features, native cupredoxins display highly positive reduction potentials compared to normal copper salts (E^0 = +159 mV vs NHE). Even though the oxidized state of the designed construct did not display the spectroscopic properties unique to native cupredoxins, the electrochemistry study revealed E^0 values that are in the range of their native counterparts. Blue copper centers, such as azurin (+308 mV at pH 7.0),[50] plastocyanin (+372 mV at pH 7.0),[51] and rusticyanin (+670 mV at pH 2.2),[30,52] have E^0 values that span from +300 to +730 mV, with the CuT1 center in laccase exhibiting a potential at the upper end of this range (at pH 5.5).[53] Green copper centers stellacyanin (+184 mV at pH 6.5)[54] and the CuT1 center in nitrite reductase (+247 mV at pH 7.2)[7,55] have lower E^0 values, with a range of +180−280 mV. A red copper center, nitrosocyanin (pH 7.0),[56] and auracyanin D (pH 7.0)[57] have the lowest E^0 of ∼80 mV. The potentials for α_3D-CR1, α_3D-CH3, and α_3D-CH4, which span from +364 to +399 mV, are comparable to reported values mentioned above and obtained from protein film electrochemistry[58,59] (Supporting Information, Table 4) for plastocyanin and azurin. Azurin has a weakly associated fifth carbonyl ligand from the peptide backbone. One of the key differences using helical bundles is that these carbonyl groups are unavailable due to H-bonding that is required to form the α-helix. Given that this extra ligand controls structure and potential, it is an important structural difference that cannot be emulated by a helical protein. However, clearly, this is not important for achieving the equivalent potential. α_3D-ChC2 possesses a higher value of +462 mV. This reduction potential is ∼200 mV lower than that of rusticyanin. This native cupredoxin has one of the highest reported E^0 values, which was attributed to its extended metal binding loop being more buried than its counterparts. In comparison to α_3D-CR1, α_3D-CH3, and α_3D-CH4, the metal binding site of α_3D-ChC2 is placed one layer toward the N-terminal end and sandwiched between apolar residues (Figure 7C), thus producing a lower dielectric environment around the copper center. Overall, these results exhibited the success of building a metal center with the proper redox property within an unrelated protein α-helical fold.

Supporting Information Table 1 compares the spectroscopic and redox properties of our designed constructs to native and CuT1 models. The absorption and EPR parameters of the core and chelate constructs match well with the corresponding characterization of CuZnSOD H120C (Cu site)[45] and Trx[BC]-4.1.1,[60] displaying a λ_{max} at ∼400 nm with R_E ratios greater than 3.0 and $A_{||}$ values greater than 120 × 10^{-4} cm^{-1}

DOI: 10.1021/acs.inorgchem.5b01330
Inorg. Chem. 2015, 54, 9470−9482

(except for the Trx, with no reported $A_{\parallel}$ value). On the basis of the CuZnSOD work,[61] which described that the rigid Zn structural site is required to achieve a CuT1 site in this native protein, the spectroscopic properties of our designed constructs indicate that the Cu(II) ion is dictating the geometry and producing tetragonal complexes. However, when the CuT1 site is buried in the core of α_3D, we observed Cu(II) properties that are much more comparable to its native counterparts and relevant designed constructs. The chelate-core construct (α_3D-ChC2) has a UV−vis spectrum that is commensurate with auracyanin D (a native CuT1 protein) and nitrosocyanin, as well as Mop23,[62] which all showed two absorbances, at ∼400 and ∼500 nm, although the respective bands for α_3D-ChC2 are about 20 and 60 nm blue-shifted. Excluding auracyanin D, these Cu(II) sites also exhibited a large $A_{\parallel}$ of (120−140) × 10^{-4} cm^{-1}. Interestingly, the UV−vis and EPR properties of Cu(II)α_3D-ChC2 have been previously observed in two CuT1 mutants, azurin M121E and rusticyanin M148E, both of which showed a brown copper complex in solution with a λ_{max} at 416 nm (2500 M^{-1} cm^{-1}) and a second less intense band at ∼550 nm (∼1000 M^{-1} cm^{-1}), as well as an increased $A_{\parallel}$ value of 90−130 × 10^{-4} cm^{-1} compared to their wild-type. Moreover, even though the Cu(II) chromophore of the core, chelate, and chelate-core constructs does not model its native counterparts as demonstrated by AM2C,[63] the reduction potentials of these constructs are comparable to those of CuT1 proteins. The $E°$ values of our constructs are higher than those of auracyanin D, nitrosocyanin, and stellacyanin by 100−200 mV and are within the range of the canonical blue copper proteins plastocyanin and azurin. Moreover, we demonstrated in this work that our CuT1 models can be attached to a surface via a Cys residues. Based on this work, future efforts could involve attaching a photoinducible chromophore to this terminal Cys to explore intramolecular and, eventually, long-range ET within the three-helix bundle of α_3D. Maybe most important, α_3D has already been modified to generate catalytic sites,[15] suggesting this is an excellent platform in which to develop a multimetallic redox enzyme.

CONCLUSIONS

De novo protein design provides a approach in studying the metal centers of native metalloproteins. Probably the most challenging objective in such studies is preparing redox-active sites, as the protein engineer must try to adapt the desired scaffold to accommodate a metal in at least two different oxidation states. This is particularly difficult with copper, as the electronic configurations confer significantly different preferences for ligand type, number, and polyhedral geometry. Thus, a structure well suited for the d^{10} Cu(I) ion may be inadequate to confer the desired structure for the d^9 Cu(II) ion. While several other groups have explored building this intriguing metal center in designed proteins, our work has attempted to transfer the center from the normal β-barrel fold to a native-like antiparallel three-α-helical motif to assess whether the unique properties of these native proteins can be retained in a three-helix bundle fold. We designed three distinct α_3D constructs: α_3D-CR, α_3D-CH, and α_3D-ChC. The CR and CH constructs produced tetragonal CuT2 Cu(II) species that displayed a dominating absorption band at ∼390 nm and hyperfine coupling constants greater than 150 × 10^{-4} cm^{-1}. Interestingly, the third design, α_3D-ChC2, produced a brown Cu(II) species similar to that which has been observed in mutated azurin and rusticyanin. This complex shows two λ_{max}, at 401 and 499 nm, yet still retains an $A_{\parallel}$ that is >70 × 10^{-4} cm^{-1} greater than azurin or plastocyanin. It also forms a relatively stable Cu(II) derivative that has a $t_{1/2}$ ≈ 3 h at room temperature. These results revealed that our designed metal binding site lacks the proper constraints to bind Cu(II) in an entatic or racked state; instead the metal ion is dictating the geometry of the complex. Nevertheless, the XAS analysis on the Cu(I) adducts showed that the designed constructs are able to reproduce structurally the reduced form of native cupredoxins, as demonstrated by their short Cu(I)−S(Cys) bond lengths of 2.16−2.23 Å. In addition, the designed constructs have a reduction potential range of +364 to +462 mV, which are comparable to their native counterparts.

We may conclude from this work that one can structurally model the Cu(I) oxidation level, but that the Cu(II) state is more challenging. It is proposed that the Cu(II) complex retains the 2HisCys ligands, but the complicating issue is that the axial ligands normally considered the weaker donors appear to have stronger interactions with the d^9 ion in these systems. Thus, this work indicates that the ability to achieve a "blue" type-1 center does not depend on providing precise control of the stronger 2HisCys donors, which we have shown can be easily achieved. Rather it requires that the chemist appropriately constrain any additional ligands to be *weaker* than they might normally be. This implies that future constructs will require more hydrophobic/steric control to restrain undesired flexibility in these scaffolds, as previously concluded by Malmström and co-workers,[47] and to select sites for mutation that do not allow for short fourth or fifth ligands from adopting a tight binding geometry. Despite these drawbacks that result from the Cu(II) oxidation level, these new metalloproteins preserve major properties, such as the proper reduction potential and coordination environment in the reduced state. These conclusions demonstrate that the β-barrel fold, while potentially important for controlling the Cu(II) structural environment, is not essential in order to form a redox center of comparable potential to CuT1 centers. Thus, these new copper proteins can serve as appropriate ET donors or acceptors of the desired potential in designed multimetallic antiparallel three-α-helical bundles that simultaneously contain an ET and a catalytic center such as found in nitrite reductase.

ASSOCIATED CONTENT

Supporting Information

The Supporting Information is available free of charge on the ACS Publications website at DOI: 10.1021/acs.inorgchem.5b01330.

CD spectra and denaturation plots of Cu(I) adducts, ^{113}Cd(II) NMR spectra, BCS titration plots, and CV and trumpet plot of each construct; an extensive table of the physical properties compared to native and designed CuT1 proteins, EXAFS analysis, and reduction potentials compared to native proteins (PDF)

AUTHOR INFORMATION

Corresponding Author

*E-mail (V. L. Pecoraro): vlpec@umich.edu.

Author Contributions

The manuscript was written through contributions of all authors. All authors have given approval to the final version of the manuscript.

DOI: 10.1021/acs.inorgchem.5b01330
Inorg. Chem. 2015, 54, 9470−9482

Funding

V.L.P. would like to thank the National Institutes of Health (NIH) for financial support for this research (ES012236), and. J.S.P. thanks the Rackham Graduate School at the University of Michigan for a research fellowship. V.L.P. and J.S.P. would also like to acknowledge the funding provided by the Chaires Internationales de Recherche Blaise Pascal.

Notes

The authors declare no competing financial interest.

■ ACKNOWLEDGMENTS

J.S.P. would like to thank the Molecular Electrochemistry Department at the University of Paris, Diderot, for allowing him to perform electrochemistry experiments. The authors would also like to thank Ms. Cathy S. Mocny, Dr. Alison G. Tebo, and Dr. Fangting Yu for collecting XAS data. Use of the Stanford Synchrotron Radiation Lightsource, SLAC National Accelerator Laboratory, is supported by the U.S. Department of Energy, Office of Science, Office of Basic Energy Sciences, under Contract No. DE-AC02-76SF00515. The SSRL Structural Molecular Biology Program is supported by the DOE Office of Biological and Environmental Research and by the National Institutes of Health, National Institute of General Medical Sciences (including P41GM103393). The contents of this publication are solely the responsibility of the authors and do not necessarily represent the official views of NIGMS or NIH.

■ REFERENCES

(1) Winkler, J. R.; Gray, H. B. *Chem. Rev.* **2014**, *114*, 3369−3380.
(2) Winkler, J. R. Long-Range Electron Transfer in Biology. *Encyclopedia of Inorganic and Bioinorganic Chemistry*; John Wiley and Sons: Chichester, U.K., 2011.
(3) Holwerda, R. A.; Wherland, S.; Gray, H. B. *Annu. Rev. Biophys. Bioeng.* **1976**, *5*, 363−396.
(4) Regan, J. J.; Di Bilio, A. J.; Langen, R.; Skov, L. K.; Winkler, J. R.; Gray, H. B.; Onuchic, J. N. *Chem. Biol.* **1995**, *2*, 489−496.
(5) Hart, P. J.; Nersissian, A. M.; George, S. D. *Encyclopedia of Inorganic and Bioinorganic Chemistry*; John Wiley and Sons: Chichester, U.K., 2011.
(6) Lu, Y. In *Comprehensive Coordination Chemistry II: From Biology to Nanotechnology*; Que, J. L., Tolman, W. B., Eds.; Elsevier Ltd.: San Diego, CA, USA, 2003; Vol. *8*, p 91.
(7) Solomon, E. I.; Szilagyi, R. K.; DeBeer George, S.; Basumallick, L. *Chem. Rev.* **2004**, *104*, 419−458.
(8) Solomon, E. I.; Hadt, R. G. *Coord. Chem. Rev.* **2011**, *255*, 774−789.
(9) Lu, Y.; Berry, S. M.; Pfister, T. D. *Chem. Rev.* **2001**, *101*, 3047−3080.
(10) Yu, F.; Cangelosi, V. M.; Zastrow, M. L.; Tegoni, M.; Plegaria, J. S.; Tebo, A. G.; Mocny, C. S.; Ruckthong, L.; Qayyum, H.; Pecoraro, V. L. *Chem. Rev.* **2014**, *114*, 3495−3578.
(11) Plegaria, J. S.; Pecoraro, V. L. *Isr. J. Chem.* **2015**, *55*, 85−95.
(12) DeGrado, W. F.; Summa, C. M.; Pavone, V.; Nastri, F.; Lombardi, A. *Annu. Rev. Biochem.* **1999**, *68*, 779−819.
(13) Walsh, S. T.; Cheng, H.; Bryson, J. W.; Roder, H.; DeGrado, W. F. *Proc. Natl. Acad. Sci. U. S. A.* **1999**, *96*, 5486−5491.
(14) Chakraborty, S.; Kravitz, J. Y.; Thulstrup, P. W.; Hemmingsen, L.; DeGrado, W. F.; Pecoraro, V. L. *Angew. Chem., Int. Ed.* **2011**, *50*, 2049−2053.
(15) Cangelosi, V. M.; Deb, A.; Penner-Hahn, J. E.; Pecoraro, V. L. *Angew. Chem., Int. Ed.* **2014**, *53*, 7900−7903.
(16) Plegaria, J. S.; Dzul, S.; Zuiderweg, E. R.; Stemmler, T. L.; Pecoraro, V. L. *Biochemistry* **2015**, *54*, 2858−2873.
(17) Luo, P.; Baldwin, R. L. *Biochemistry* **1997**, *36*, 8413−8421.
(18) Rohl, C. A.; Baldwin, R. L. *Biochemistry* **1997**, *36*, 8435−8442.
(19) Santoro, M. M.; Bolen, D. W. *Biochemistry* **1988**, *27*, 8063−8068.
(20) Golombek, A. P.; Hendrich, M. P. *J. Magn. Reson.* **2003**, *165*, 33−48.
(21) Xiao, Z.; Loughlin, F.; George, G. N.; Howlett, G. J.; Wedd, A. G. *J. Am. Chem. Soc.* **2004**, *126*, 3081−3090.
(22) McMaster, W. H.; Del Grande, N. K.; Mallett, J. H.; Hubbell, J. H. *Compilation of X-Ray Cross Sections*; Lawrence Livermore National Laboratory Report, 1969.
(23) Weng, T. C.; Waldo, G. S.; Penner-Hahn, J. E. *J. Synchrotron Radiat.* **2005**, *12*, 506−510.
(24) George, G. N.; Pickering, I. J. *EXAFSPAK*, Stanford Synchrotron Radiation Laboratory: Menlo Park, CA, 2000.
(25) Rehr, J. J.; Kas, J. J.; Vila, F. D.; Prange, M. P.; Jorissen, K. *Phys. Chem. Chem. Phys.* **2010**, *12*, 5503−5513.
(26) Dimakis, N.; Bunker, G. *Phys. Rev. B: Condens. Matter Mater. Phys.* **2002**, *65*, 201103-1−201103-4.
(27) Chen, Y. H.; Yang, J. T.; Chau, K. H. *Biochemistry* **1974**, *13*, 3350−3359.
(28) Ghosh, D.; Pecoraro, V. L. *Inorg. Chem.* **2004**, *43*, 7902−7915.
(29) Karlsson, B. G.; Tsai, L. C.; Nar, H.; Sanders-Loehr, J.; Bonander, N.; Langer, V.; Sjolin, L. *Biochemistry* **1997**, *36*, 4089−4095.
(30) Hall, J. F.; Kanbi, L. D.; Strange, R. W.; Hasnain, S. S. *Biochemistry* **1999**, *38*, 12675−12680.
(31) Kitajima, N. In *Advances in Inorganic Chemsitry*; Elsevier, Ltd.: Dordrecht, Amsterdam, 1992; Vol. *39*, pp 1−77.
(32) Siluvai, G. S.; Mayfield, M.; Nilges, M. J.; Debeer George, S.; Blackburn, N. J. *J. Am. Chem. Soc.* **2010**, *132*, 5215−5226.
(33) Öz, G.; Pountney, D. L.; Armitage, I. M. *Biochem. Cell Biol.* **1998**, *76*, 223−234.
(34) Engeseth, H. R.; McMillin, D. R.; Otvos, J. D. *J. Biol. Chem.* **1984**, *256*, 4822−4826.
(35) Marks, J.; Pozdnyakova, I.; Guidry, J.; Wittung-Stafshede, P. *JBIC, J. Biol. Inorg. Chem.* **2004**, *9*, 281−288.
(36) Kau, L. S.; Spira-Solomon, D. J.; Penner-Hahn, J. E.; Hodgson, K. O.; Solomon, E. I. *J. Am. Chem. Soc.* **1987**, *109*, 6433−6442.
(37) Chen, K.; Yuldasheva, S.; Penner-Hahn, J. E.; O'Halloran, T. V. *J. Am. Chem. Soc.* **2003**, *125*, 12088−12089.
(38) DeBeer, S.; Wittung-Stafshede, P.; Leckner, J.; Karlsson, G.; Winkler, J. R.; Gray, H. B.; Malmström, B. G.; Solomon, E. I.; Hedman, B.; Hodgson, K. O. *Inorg. Chim. Acta* **2000**, *297*, 278−282.
(39) DeBeer George, S.; Basumallick, L.; Szilagyi, R. K.; Randall, D. W.; Hill, M. G.; Nersissian, A. M.; Valentine, J. S.; Hedman, B.; Hodgson, K. O.; Solomon, E. I. *J. Am. Chem. Soc.* **2003**, *125*, 11314−11328.
(40) Basumallick, L.; Sarangi, R.; DeBeer George, S.; Elmore, B.; Hooper, A. B.; Hedman, B.; Hodgson, K. O.; Solomon, E. I. *J. Am. Chem. Soc.* **2005**, *127*, 3531−3544.
(41) Leger, C.; Bertrand, P. *Chem. Rev.* **2008**, *108*, 2379−2438.
(42) Laviron, E. *J. Electroanal. Chem. Interfacial Electrochem.* **1979**, *101*, 19−28.
(43) Solomon, E. I. *Inorg. Chem.* **2006**, *45*, 8012−8025.
(44) Lu, Y.; Gralla, E. B.; Roe, J. A.; Valentine, J. S. *J. Am. Chem. Soc.* **1992**, *114*, 3560−3562.
(45) Lu, Y.; Roe, J. A.; Bender, C. J.; Peisach, J.; Banci, L.; Bertini, I.; Gralla, E. B.; Valentine, J. S. *Inorg. Chem.* **1996**, *35*, 1692−1700.
(46) Malmström, B. G. *Eur. J. Biochem.* **1994**, *223*, 711−718.
(47) Wittung-Stafshede, P.; Hill, M. G.; Gomez, E.; Di Bilio, A. J.; Karlsson, B. G.; Leckner, J.; Winkler, J. R.; Gray, H. B.; Malmström, B. G. *JBIC, J. Biol. Inorg. Chem.* **1998**, *3*, 367−370.
(48) Walsh, S. T. R.; Lee, A. L.; DeGrado, W. F.; Wand, A. J. *Biochemistry* **2001**, *40*, 9560−9569.
(49) Karlsson, B. G.; Tsai, L. C.; Nar, H.; Sanders-Loehr, J.; Bonander, N.; Langer, V.; Sjolin, L. *Biochemistry* **1997**, *36*, 4089−4095.
(50) Pascher, T.; Karlsson, B. G.; Nordling, M.; Malmström, B. G.; Vanngard, T. *Eur. J. Biochem.* **1993**, *212*, 289−296.
(51) Anderson, G. P.; Sanderson, D. G.; Lee, C. H.; Durell, S.; Anderson, L. B.; Gross, E. L. *Biochim. Biophys. Acta, Bioenerg.* **1987**, *894*, 386−398.

DOI: 10.1021/acs.inorgchem.5b01330
Inorg. Chem. 2015, 54, 9470−9482

(52) Lappin, A. G.; Lewis, C. A.; Ingledew, W. J. *Inorg. Chem.* **1985**, *24*, 1446−1450.
(53) Xu, F.; Berka, R. M.; Wahleithner, J. A.; Nelson, B. A.; Shuster, J. R.; Brown, S. H.; Palmer, A. E.; Solomon, E. I. *Biochem. J.* **1998**, *334*, 63−70.
(54) Sailasuta, N.; Anson, F. C.; Gray, H. B. *J. Am. Chem. Soc.* **1979**, *101*, 455−458.
(55) Olesen, K.; Veselov, A.; Zhao, Y.; Wang, Y.; Danner, B.; Scholes, C. P.; Shapleigh, J. P. *Biochemistry* **1998**, *37*, 6086−6094.
(56) Arciero, D. M.; Pierce, B. S.; Hendrich, M. P.; Hooper, A. B. *Biochemistry* **2002**, *41*, 1703−1709.
(57) King, J. D.; McIntosh, C. L.; Halsey, C. M.; Lada, B. M.; Niedzwiedzki, D. M.; Cooley, J. W.; Blankenship, R. E. *Biochemistry* **2013**, *52*, 8267−8275.
(58) Andolfi, L.; Bruce, D.; Cannistraro, S.; Canters, G. W.; Davis, J. J.; Hill, H. A. O.; Crozier, J.; Verbeet, M. P.; Wrathmell, C. L.; Astier, Y. *J. Electroanal. Chem.* **2004**, *565*, 21−28.
(59) Jeuken, L. J. C.; Armstrong, F. A. *J. Phys. Chem. B* **2001**, *105*, 5271−5282.
(60) Hellinga, H. W. *J. Am. Chem. Soc.* **1998**, *120*, 10055−10066.
(61) Lu, Y.; Lacroix, L. B.; Lowery, M. D.; Solomon, E. I.; Bender, C. J.; Peisach, J.; Roe, J. A.; Gralla, E. B.; Valentine, J. S. *J. Am. Chem. Soc.* **1993**, *115*, 5907−5918.
(62) Schnepf, R.; Haehnel, W.; Wieghardt, K.; Hildebrandt, P. *J. Am. Chem. Soc.* **2004**, *126*, 14389−14399.
(63) Shiga, D.; Nakane, D.; Inomata, T.; Funahashi, Y.; Masuda, H.; Kikuchi, A.; Oda, M.; Noda, M.; Uchiyama, S.; Fukui, K.; Kanaori, K.; Tajima, K.; Takano, Y.; Nakamura, H.; Tanaka, T. *J. Am. Chem. Soc.* **2010**, *132*, 18191−18198.

DOI: 10.1021/acs.inorgchem.5b01330
Inorg. Chem. 2015, 54, 9470−9482